Pressure-induced phase transitions in amorphous and metastable crystalline germanium by Raman scattering, x-ray spectroscopy, and *ab initio* calculations

F. Coppari,[1] J. C. Chervin,[1] A. Congeduti,[2] M. Lazzeri,[1] A. Polian,[1] E. Principi,[3] and A. Di Cicco[1,3]
[1]*IMPMC-CNRS UMR 7590, Université P. et M. Curie, 140 rue de Lourmel, 75015 Paris, France*
[2]*Synchrotron Soleil, L'Orme des Merisiers, St. Aubin, 91192 Gif-sur-Yvette, France*
[3]*CNISM, Dipartimento di Fisica, Università di Camerino, Via Madonna delle Carceri, Camerino, 62032 Madonna delle Carceri, Italy*
(Received 18 February 2009; revised manuscript received 17 July 2009; published 23 September 2009)

A detailed study of the pressure-induced phase transitions in amorphous Ge (*a*-Ge) up to 17 GPa is reported combining Raman scattering, x-ray absorption spectroscopy (XAS) measurements, and density-functional theory calculations. *a*-Ge samples were films obtained by evaporation and characterized by different density of voids. Specific and reproducible phase transitions (interpreted as disorder-disorder, disorder-order, and order-disorder) are observed on pressurization and depressurization, depending on the initial density of voids. Details of the structural and vibrational properties of the various phases have been obtained by XAS and Raman-scattering data analysis. Samples showing a low density of voids transform first into a metallic disordered phase (8 GPa) and to GeII at higher pressures while those with higher density of voids transform directly to the GeII phase (10.6 GPa). Upon depressurization, the first nucleates into the GeIII metastable phase in the 7.2–2.3 GPa pressure range, while the others return to the amorphous state below 5 GPa. The behavior upon depressurization shows that the initial morphology determines the transitions experienced by the pressurized sample down to ambient pressure.

DOI: 10.1103/PhysRevB.80.115213 PACS number(s): 61.43.Dq, 64.70.−p, 78.30.Ly, 78.70.Dm

I. INTRODUCTION

Silicon- and germanium-based semiconductors have been studied in the last decades using a variety of experimental and theoretical methods being materials of outmost importance in basic science and applications in everyday life. Nevertheless, detailed and unambiguous understanding of the complex phenomena taking place in amorphous specimens upon application of an external pressure is not yet available. In particular, pure germanium is a IV group semiconductor which is known to show a complex behavior upon pressurization and depressurization. At ambient pressure, the stable phase is the diamond structure (GeI), where each Ge atom is surrounded by four neighbors in a tetrahedral symmetry (fcc structure with two atoms per unit cell). Upon application of pressure, the tetrahedral bonding network is broken and the number of neighbors and the density increase. Around 11 GPa, a transition to the metallic β-Sn structure (GeII) occurs. Upon decompression, the crystalline stable structure is not always recovered, rather metastable crystalline phases are observed. The most common one is called ST12 (GeIII). It is based on tetrahedral structure with 12 atom per unit cell arranged to form fivefold and sevenfold rings [space group $P4_32_12(D_4^8)$].[1] In this phase, Ge has higher density (about 10%) than the underlying stable one as reported in Ref. 2. Despite the existence of this, metastable phase is known since 1960s[2] and a great number of experiments has been performed since there, a clear identification and assignments of Raman peaks is still lacking, as also shown in recent experimental studies where the metastable crystalline phase was obtained through indentation technique.[3–7] As highlighted in previous works, the major problems come from the competition between different metastable phases, in which germanium can crystallize. As reported in Ref. 8 in case of rapid decompression (about 1 s from the high-pressure phase), a cubic structure characterized by eight atoms per unit cell and called BC8 (or GeIV) (Refs. 8 and 9) is likely to occur. This structure is not stable at room temperature but it transforms to the lonsdaleite structure (hexagonal with four atoms per unit cell) within a few hours.

The local structure of the amorphous form of Ge (*a*-Ge) at ambient conditions is quite similar to crystalline one (GeI). It is tetrahedrally bonded. Bond lengths do not differ more than 1% from the crystalline form and bond angles show a modest spread of the order of 10 degrees about the ideal value. As its crystalline counterpart, *a*-Ge shows a complex behavior when an external pressure is applied, and scattered results are reported in literature. In particular, evidence for a sharp drop in resistivity and crystallization of thin *a*-Ge films[10,11] was found at about 6 GPa. The x-ray absorption spectroscopy (XAS) technique was used to study the evolution of the local structure at high pressures. Freund *et al.*[12] showed that *a*-Ge remains amorphous up to 8.9 GPa while more recent XAS measurements[13] showed that at 8 GPa *a*-Ge undergoes a phase transition though remaining amorphous. The glass transitions in Si and Ge under pressure were also studied in two recent works both experimentally[14,15] and through molecular dynamic simulations.[16] The combination of Raman and XAS spectroscopy measurements permitted us to confirm that 8 GPa marks the onset of a polyamorphic transition in our more homogeneous samples.[17] Moreover, Ref. 17 demonstrates that the actual transitions observed in a given sample depend on the initial morphology of the sample. However, the experiments reported in Ref. 17 were done in a limited pressure range (10–12 GPa) and did not account for the transitions occurring upon depressurization.

Here, we report the results and the interpretation of detailed Raman-scattering and XAS experiments at high pressure of *a*-Ge. This work is aimed to investigate pressure-induced phase transition, addressing the question of the

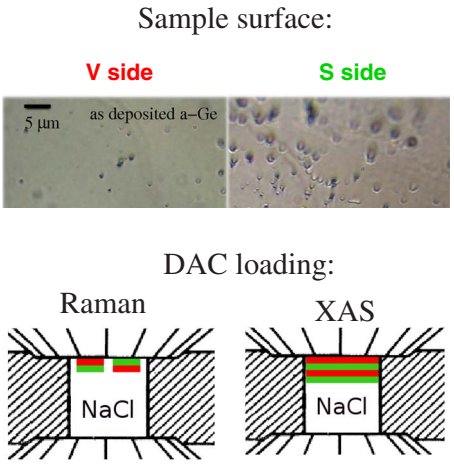

FIG. 1. (Color online) Upper figures: images of the sample surfaces obtained by an optical metallographic microscope. It is evident that the two surfaces of the deposition are characterized by a different density of voids. In particular, the one exposed to the vacuum (*V* side) is more homogeneous, while the one in contact with the substrate (*S* side) shows a higher density of defects. Bottom figures: sketch of the loading of the high-pressure (DAC) for Raman-scattering and XAS measurements. Different gray levels (print version) correspond to the two surfaces (red or darker gray is used for *V* side and green or lighter gray for *S* side). The sample was kept in contact with diamonds by NaCl, used as pressure transmitting medium. DAC was also loaded with a ruby for pressure measurements.

occurrence of polyamorphism and metastability upon compression and decompression cycles. The Raman-scattering experiments of the solid metastable phases obtained upon decompression are interpreted using density-functional theory calculations. The peculiar behavior under pressure of samples with different density of voids is examined in details by studying their local structural and vibrational properties using state-of-the-art techniques.

II. METHODOLOGICAL APPROACHES

A. Sample preparation and characterization

Amorphous germanium (*a*-Ge) was obtained by evaporation of high-purity crystalline Ge over a cleaned and degassed glass substrate at ambient temperature and in vacuum conditions (10^{-6} mbar). Deposition rate was about 2 Å/s and a thickness of about 3 μm was reached (both parameters were monitored by a calibrated quartz-crystal oscillator).

X-ray diffraction measurements confirmed that the deposited film was amorphous. A careful examination using electron and optical microscopies was performed (see also Ref. 17). It showed that sample is characterized by a certain amount of defects and that their density is different according to the surface (upper part of Fig. 1). The surface in contact with the glass substrate (*S* side) during the deposition is darker and characterized by a larger amount of voids (around 5.8%), while the one on the vacuum side (*V* side) is more reflective and has a lower density of defects (around 1%).

B. Raman measurements

Raman spectra of *a*-Ge under high-pressure conditions were collected. Diamond anvil cell (DAC) with 800 μm flat surface was used as pressure device. A Cu-Be gasket was filled with small sample flakes showing the two surfaces, together with NaCl as pressure-transmitting medium. NaCl is known to present problems of hydrostaticity especially at very high pressure conditions. Nevertheless, it proved to be the best choice due to the need of dissipating the heat load (caused by laser radiation) avoiding crystallization. In order to exclude effect of nonhydrostaticity on the onset of phase transitions, Raman measurements on crystalline Ge (not affected by laser heating) were performed using two different transmitting media, notably NaCl and a more hydrostatic one, Ne, loaded at about 1.5 kbar. A 400 μm culets cell and a stainless-steel gasket were used in both cases. No noticeable differences in the Raman spectra and phase transitions onsets were observed using those two pressure-transmitting media up to about 12 GPa. In all Raman and XAS experiments, pressure was measured via ruby fluorescence technique.[18]

A typical sketch of the sample assembly for Raman measurements, allowing measurements of both surface types of the samples, is shown in the lower-left part of Fig. 1. Raman spectra were collected with the 514.5 nm line from an argon-ion laser using up to 750 mW (for *a*-Ge sample) and 250 mW (for GeI sample) of nominal power at the laser exit. The light was focused on a spot of about 2 μm at the sample surface. The effective power incident on the sample inside the DAC was measured to be roughly 20 times smaller then the one at the laser exit. Spectra of *a*-Ge were usually recorded using a total integration time of 4000 s, repeating the scans up to 12 times in the frequency range 0–650 cm^{-1}. Spectra of crystalline GeI and GeIII samples were obtained integrating 600 and 1800 s, respectively (repeated 2–4 times). Raman spectra were collected from ambient pressure up to about 15 GPa performing several pressure cycles as discussed below and reported also in Ref. 19.

C. XAS data

High-pressure x-ray absorption measurements on amorphous Ge were performed at the new dispersive XAS ODE beamline at Soleil synchrotron-radiation facility. Spectra were collected at Ge *K* edge (11 keV) in the range 0–17 GPa using diamond-anvil cell of 400 μm culets. Inconel gasket hole was filled with *a*-Ge sample, NaCl as pressure transmitting medium, and a ruby for pressure measurement. In order to improve the signal, gasket hole was completely filled with several layers of *a*-Ge films (see lower right of Fig. 1) in order to have a homogeneous thickness (6–9 μm for our experiments). We performed two sessions of high-pressure XAS measurements using also an image-plate detector MAR345 and a single-wavelength setup to collect x-ray diffraction patterns in the same experimental conditions. A typical Ge *K*-edge XAS spectrum of *a*-Ge is reported in Fig. 2.

Raw XAS spectra as recorded by the charge coupled device (CCD) detector must be calibrated using reference spectra collected on a reliable energy scale. In our case, energy calibration was performed using a *a*-Ge spectrum collected using a Si(331) channel-cut monochromator (D42 beamline at LURE, Orsay, France[20]). In Fig. 2, we show the compari-

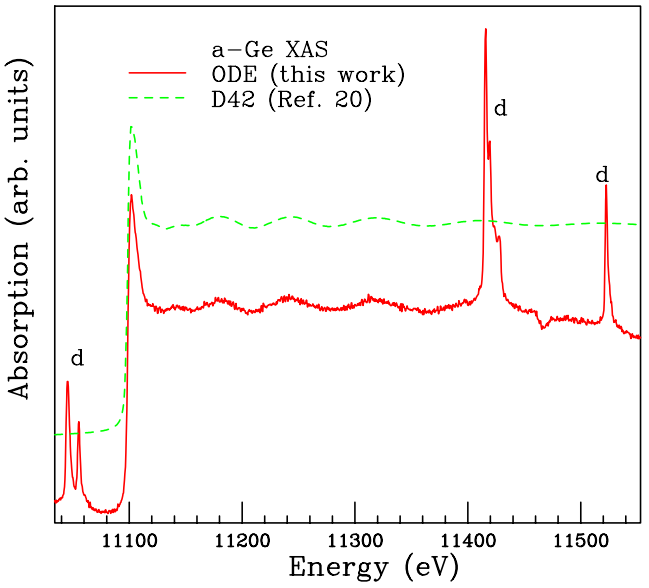

FIG. 2. (Color online) *K*-edge XAS spectra of amorphous germanium. The spectrum represented by a green dashed line was collected at D42 beamline (LURE) (Ref. 20) and has been used as reference spectrum for energy calibration. The continuous red line represents our first (DAC membrane at ambient pressure) spectrum collected during the measurements described in this work (ODE beamline, Soleil Synchrotron). The sharp peaks indicated by the label "d" are Bragg peaks assigned to the diamonds of the high-pressure cell.

son between the reference spectrum and the one obtained after loading the high-pressure cell (DAC membrane at ambient pressure). The presence of Bragg peaks due to the diamonds (peaks indicated as "d" in Fig. 2) reduces the usable energy range, although in our experiment, the cell was oriented in order to optimize the positions of the peaks and to minimize their number.

A first calibration was done using XAS spectra and was further refined using XAS signal oscillations. The relation between energy and pixel number was found to be almost linear: $E=a+bn+cn^2+dn^3$, with $a=11\,012.4$ eV, $b=0.3185\,47$ eV, $c=2.577\,07\times10^{-4}$ eV, and $d=-1.475\,06\times10^{-7}$ eV.

XAS data analysis was performed using GNXAS package (see Refs. 21 and 22 and references therein). The basic assumption within the GNXAS method for data analysis is that it is possible to account for the structural signal by adding a finite number of contributions associated with well-defined peaks of the pair $[g_2(r)]$, three-body $[g_3(r)]$, and four-body $[g_4(r)]$ distribution functions (see Refs. 21 and 22 and references therein). The program computes a model absorption signal $a_m(E)$ by adding to the structural oscillations $\chi_m(k)$ a suitable background model. The signal is compared and refined directly on the experimental absorption spectrum $a(E)$.

In our analysis, the theoretical $\chi(k)$ signal was reconstructed using a simple first-shell model. The total signal due to a specified $g_2(r)$ peak, defined as the irreducible two-body signal $\gamma^{(2)}$, is calculated considering single- and multiple-scattering contributions ($\gamma^{(2)}=\chi_2+\chi_4$). During the fitting procedure, the values of the parameters specifying the $g_2(r)$ peak (modeled with a Gaussian function), notably the average interatomic distance (R) and their variance (σ^2), were refined. Values of the structural parameters at different pressures are reported in Fig. 9.

D. Density functional theory simulations

We computed the zero-momentum phonon frequencies of ST12 and BC8 crystalline phases of germanium from first principles within density-functional theory (DFT).[23,24] This calculation was performed in order to understand some features of the measured vibrational Raman spectra and identify the metastable phases obtained experimentally. The phonon frequencies were computed using the approach described in Ref. 25. Calculations were done with the PWSCF-PHONON codes[26] within the pseudopotential and plane-waves approaches. We used norm-conserving pseudopotential,[27] with a core radius of 2.0 a.u. for the 4*s* and 4*p* electrons, and an energy cutoff of 60 Ry for the plane waves. The exchange-correlation functional was described by the generalized-gradient approximation (GGA) of Ref. 28 since GGA is known to be accurate for germanium.[29]

As a first check, we computed the equilibrium lattice spacing and optical-phonon frequency for GeI (diamond structure), finding, respectively, $a_0=5.66$ Å and $\omega_0=292$ cm^{-1}, in good agreement with the measured values of $a_0=5.66$ Å and $\omega_0=300.6\pm0.5$ cm^{-1}.[30,31] The calculations for ST12 and BC8 were done using the lattice structure deduced by previous experimental works.[32] For ST12, we used an electronic integration mesh of $7\times7\times7$ k points, finding an electronic gap of 475 meV at the point $q=(0.36,0.36,0)$ Å^{-1}. Calculations for different pressures were done considering the experimental lattice spacings taken from Ref. 30 without changing the positional parameters.

For BC8-Ge, we used a $10\times10\times10$ electronic mesh. Since BC8 is semimetallic, we used the smearing approach of Ref. 33 (with smearing of 0.02 Ry). The phonon frequencies obtained with these parameters are well converged for both ST12 and BC8 phases.

The zero-momentum frequencies determine the energies of the peaks observed in a vibrational Raman experiment. For ST12, we also computed the DFT Raman tensor following the method of Ref. 34. The Raman tensor was then used to determine the intensities and, thus, to simulate the Raman spectra, following the standard procedure based on the Placzek approximation.[35] The ST12 Raman tensor was calculated with a $12\times12\times12$ electronic mesh. The theoretical Raman spectra were then obtained by considering a uniform smearing of 2 cm^{-1}. We remark that the Placzek approximation is strictly valid in the nonresonant regime that is when the energy of the incident laser is much smaller than the electronic gap.[35] In the present situation (the laser energy is 2410 meV and the estimated gap is 475 meV), electronic resonance effects could affect the actual value of the Raman intensities. However, we consider that the present calculations can still give a qualitative indication of the relative intensity of the Raman peaks. For BC8, it was not possible to compute the Raman tensor since it is a semimetal.

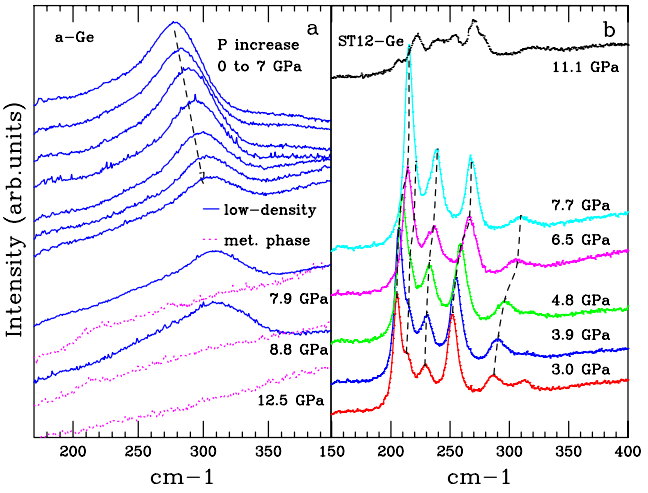

FIG. 3. (Color online) (a) Experimental Raman spectra of *a*-Ge for increasing pressure. Around 8 GPa, the Raman *a*-Ge band at about 300 cm^{-1} is lost in *V* side sample (dot line), while *S* side remains amorphous till about 10 GPa (continuous line). At about 12.5 GPa, no evidence for any Raman signal above the background is observed. (b) Raman spectra of metastable Ge (ST12) at different pressures. Spectra are characterized by five peaks between 150–350 cm^{-1}. Metastability is observed in a wide range of pressure, notably 3–11 GPa, considering several downloading and reloading pressures.

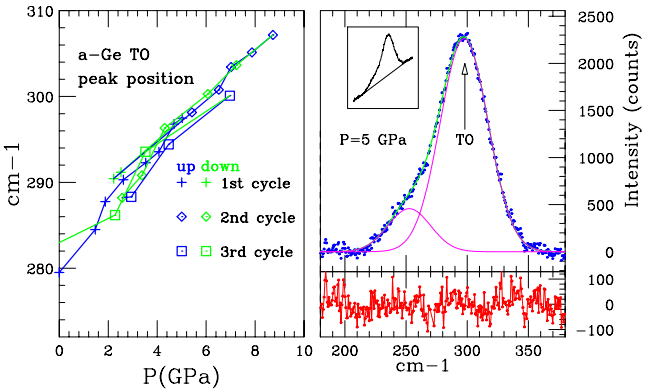

FIG. 4. (Color online) Left panel: shift of the Raman TO band of low-density *a*-Ge upon pressurization and depressurization cycles (blue and green, respectively, different symbols for each cycle) up to about 9 GPa. At higher pressures, the Raman signal on both sides *V* and *S* is lost due to metallization. The trend upon several pressure cycles is reproducible on both sides. Right panel: raw *a*-Ge Raman data at 5 GPa (inset) compared to a best-fit curve resulting from a decomposition into two Gaussian peaks (the more important one corresponds to the TO vibrational band). The residual curve on a magnified scale is shown at the bottom.

III. RESULTS AND DISCUSSION

A. Raman-scattering experiments

The trend of Raman-scattering spectra upon increasing pressure is discussed in Ref. 17. Here we recall that at ambient pressure Raman spectrum of *a*-Ge presents a bump at 279 cm^{-1} and its shift as a function of pressure is shown in Fig. 3(a). $P=7.9$ GPa marks the onset of a transition to a metallic phase which involves only the sample with low density of voids (*V* side). This phase is characterized by an almost complete loss of Raman-scattering signal and higher reflectivity. In the *S* side sample (high density of voids), the characteristic Raman broad peak of *a*-Ge is present till 10.6 GPa. No further differences in the spectra of the *V* and *S* side samples were observed by increasing pressure up to about 12.5 GPa, where a complete loss of visible Raman-scattering peaks is found (see bottom curve in Fig. 3).

As reported in Ref. 36, the Raman spectrum of low-density *a*-Ge is characterized by two main bands: the first near the frequency of the GeI Raman peak (300.6 cm^{-1}) due to vibrational optical modes[31] and the second below 100 cm^{-1}. The broadening of those bands corresponds to the broadening of the vibrational density of states in the amorphous material. In our experimental spectra, only the first band was studied because low-frequency features were masked by the presence of sharp plasma peaks of the laser. The band shift upon increasing pressure was studied by using a fitting procedure based on a two peaks model, in which the shape of the band was decomposed considering a main Gaussian peak due to transverse optical (TO) modes of vibration and a contribution of the other modes responsible for the shoulder at lower frequencies (Fig. 4, right). This band shifts to higher frequencies as a function of increasing pressure, as shown by the variation of the peak position associated with the TO vibrational modes, reported in Fig. 4 (left). We notice that the shift of the TO peak is quite reproducible upon various pressure cycles and for both sides *V* and *S* wherever the low-density amorphous phase is present (see the three cycles in Fig. 4).

The new data reported here concern mainly the behavior of the sample upon depressurization. We performed several cycles of pressurization and depressurization discussed in more details in Ref. 19. During these experiments, we have verified that the behavior of the two sides *V* and *S* of the sample upon depressurization from the metallic phases is different.

In particular, the *V* side of the sample transforms to a crystalline metastable phase at 7.2 GPa. Its Raman spectrum shows five peaks in the frequency range 150–350 cm^{-1} [Fig. 3(b)] which shift to lower frequencies as a function of decreasing pressure. The peak at about 310 cm^{-1}, which appears in the lower-pressure spectrum, is assigned to the TO vibrational mode characteristic of stable GeI (Fig. 5).[36] The lowest-pressure spectrum containing signature of the ST12 structure was collected at about 2.3 GPa. Once the diamond cell is open (ambient pressure), the amorphous structure is recovered. On the other hand, the *S* side sample does not undergo recrystallization upon downloading pressure, but transforms directly back to the amorphous phase around 5 GPa and this structure is maintained even at ambient conditions.

In order to verify possible effects on the observed *a*-Ge transitions due to the choice of the pressure transmitting medium and cell loading conditions, we performed high-pressure Raman-scattering experiments under similar conditions on chunks of ultrapure crystalline GeI. These experiments showed that in the range of 0–15 GPa, pressure

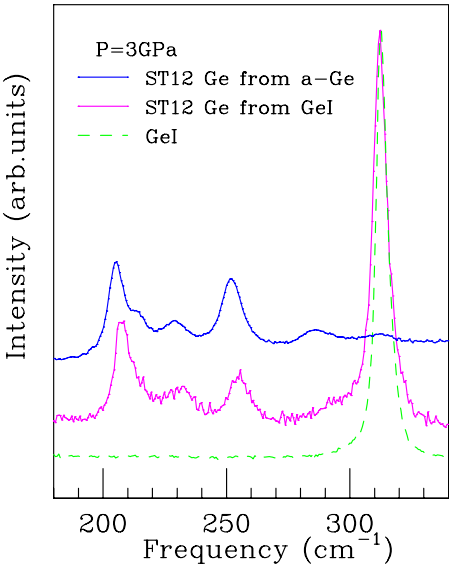

FIG. 5. (Color online) Raman pattern of the ST12 (GeIII) starting from both *a*-Ge (upper, blue line) and GeI (middle curve, magenta) collected at about 3 GPa. The characteristic GeI optical vibrational mode, shown in the figure (bottom dashed curve, green), is also present in the Raman patterns assigned to the metastable ST12 phase (being the main peak in the pattern obtained from the original crystalline sample).

values of phase transitions are not affected by the choice of the pressure-transmitting medium (differences being of the order of 0.5 GPa between Ne and NaCl). Our measurements showed also, in agreement with previous studies,[30,37] that transitions do not take place abruptly, but there is a pressure range of about 2–3 GPa (for GeI-GeII and GeII-GeIII transitions, respectively) of coexistence of phases. Pressure value for the onset of GeI-GeII transition (around 11 GPa) is in good agreement with values reported in literature, even if the complete transition is achieved near about 14 GPa. For what concerns the occurrence of the GeIII phase upon depressurization of an originally crystalline sample, we show in Fig. 5 a comparison of Raman scattering for various samples measured at 3 GPa. The Raman patterns obtained depressurizing both amorphous and crystalline samples show the same vibrational modes, typical of the ST12 structure as discussed below. The GeI TO mode, shown for comparison in Fig. 5, is also observed in the pattern of the depressurized samples. This is interpreted as due to a partial crystallization into the stable phase, much more important for the sample which was originally an ultrapure GeI crystal.

The spectra of the metastable crystalline phase obtained upon decompression have been studied on the basis of the first-principles calculations described in Sec. II D. In Fig. 6, we compare the Raman spectrum at 3 GPa [see also Fig. 3(b), bottom] with our first-principles calculations for the crystalline ST12 and BC8 structures at ambient conditions. We notice that the calculated spectrum for ST12-Ge shows eight Raman-active peaks in the frequency range 150–300 cm^{-1}, the most intense being in qualitative agreement with the experimental one. In the same range, BC8 has five phonon frequencies. Following symmetry arguments,[38] the frequency at 213 cm^{-1} (blue dashed line) is not Raman

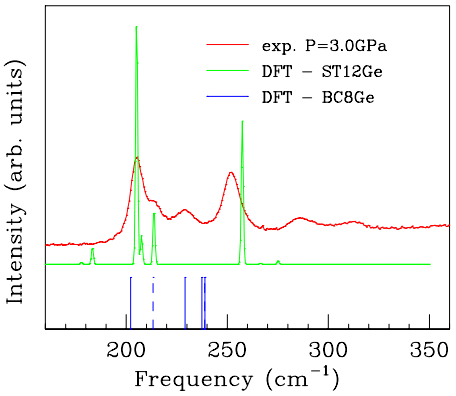

FIG. 6. (Color online) Comparison between the experimental Raman spectrum at 3 GPa, obtained on the *V* side of the *a*-Ge sample, and the simulated spectrum for ST12 structure at ambient conditions. Calculated phonon frequencies for the BC8 structure are also reported. The mode corresponding to the phonon frequency indicated by a dashed line is not Raman active.

active. On the basis of the comparison shown in Fig. 6, we conclude that the vibrational spectrum is compatible with that of the ST12 phase. This assignment is supported also by the results of the parallel x-ray absorption and diffraction experiments (see Sec. III B).

ST12 Raman spectra have been also calculated at different pressures. In Fig. 7, the theoretical and experimental phonon frequencies as a function of pressures are shown. The experimental vibrational frequencies found in this work are depicted as filled circles and their slope as a function of pressure is in very good agreement with the results of our calculations, reported as continuous lines (green color). It is important to remark that present results are in good agreement with previous ones obtained using crystalline Ge, notably with those of Ref. 39 (crosses in Fig. 7) and partially with those of Ref. 40 (dashed lines in Fig. 7).

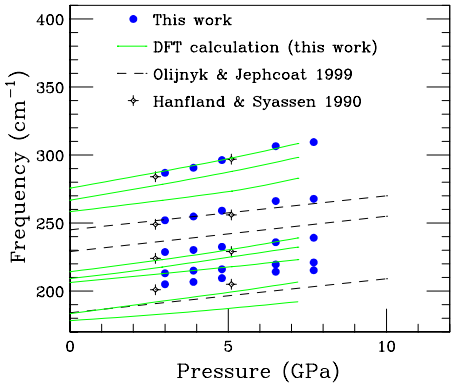

FIG. 7. (Color online) Comparison between phonon frequencies at different pressures as obtained by our measurements (blue circles) and theoretical calculations (continuous lines). A comparison to experimental works of Olijnyk and Jephcoat (Ref. 40) (dashed line) and Hanfland and Syassen (crosses) (Ref. 39) is also reported. Our experimental frequencies are in good agreement with those of Ref. 39.

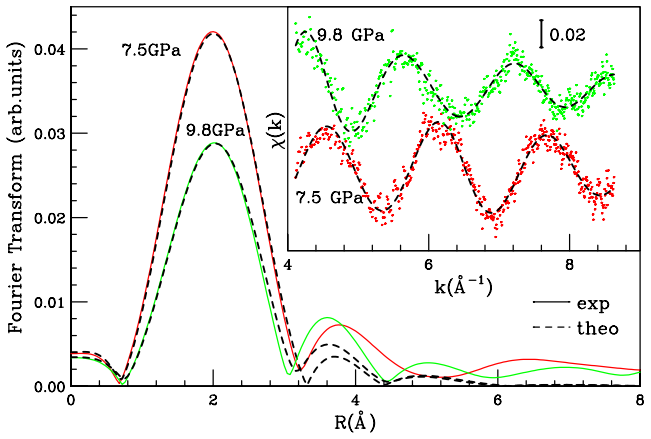

FIG. 8. (Color online) Fourier transforms and XAS signals (inset) of sample before and after the metallization onset (around 8 GPa). Raw XAS spectra and FT patterns are shown as red (7.5 GPa) and green (9.8 GPa) lines (FT) and dots (XAS). Best-fit curves obtained by GNXAS data analysis are shown as dashed black lines.

B. XAS measurements

XAS experiments at high pressure allowed us to investigate changes in the local structure occurring on our *a*-Ge sample and the metallization onset. As reported in Ref. 17, a proof of the metallic character of the new phase has been obtained by looking at the shift of the Ge *K*-edge position at high pressure. The transition observed at about 8 GPa was associated with the occurrence of a low-density (LDA) to high-density amorphous (HDA) phase transition. In this work, we include the results of our new XAS measurements where higher-pressure values were reached (17 GPa), giving more details on the behavior upon downloading pressure. XAS measurements were found to confirm the pressure onsets for the transitions obtained by Raman-scattering experiments. In our previous work,[17] we showed that the Fourier transform (FT) of the XAS spectra shows a dramatic drop in the intensity of the first peak at 8 GPa followed by an increase around 10 GPa. In Fig. 8, we report the comparison of the FTs and of the XAS spectra before and after the metallization onset. The dramatic change in the XAS oscillation frequency due to the phase transition can be appreciated in the inset, while the intensity change is monitored by the height of the FT peak. The accuracy of the single-shell fitting (dashed lines in Fig. 8) obtained using GNXAS (see Sec. II C) is evident by looking both at the XAS and FT patterns.

The first-neighbor distribution associated with the FT first peak has been analyzed using GNXAS package[20] using a single-shell model in a wide pressure range 0–17 GPa. The results of this data analysis are reported in Fig. 9. The trend of the mean first-neighbor distance R and variance σ^2 for our whole set of measurements along both pressurization and depressurization cycles are shown. Two separate XAS experiments (diamonds and crosses) gave the same structural results and transition onsets within the experimental uncertainty as shown in Fig. 9. XAS data upon the depressurization have been collected and analyzed once the phase transition from the high-pressure metallic phase was completed.

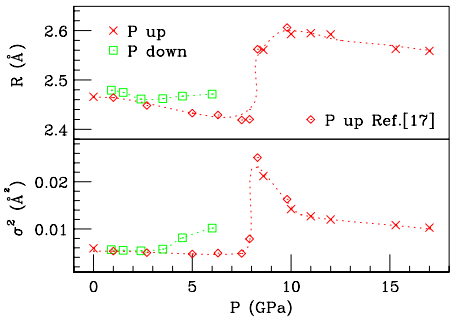

FIG. 9. (Color online) Structural parameters as a function of pressure, as obtained by XAS data analysis. Both previous measurements (Ref. 17) (diamonds, red) for increasing pressure and present ones obtained upon pressurization and depressurization are shown (crosses). In the upper panel values of mean interatomic distances (R) are reported. By increasing pressure, the initial value of 2.466 Å obtained at ambient pressure decreases up to the onset of the polyamorphic transition, where a sudden increase occurs. After the transition, its value tends to decrease as a consequence of the compression. The behavior of bond variances (σ^2) is similar: at 8 GPa, its sharp increase is associated with higher structural disorder. Around 10 GPa, its value decreases, indicating a more ordered structure. Upon pressure download (crosses, green), both σ^2 and R values gradually returns to the starting ones. Typical errors in the first-neighbor distances R and bond variances σ^2 are 0.005 Å and $\frac{\Delta\sigma^2}{\sigma^2} \sim 10\%$. Coordination numbers (CNs) were kept fixed during refinement (4 for the LDA phase and upon depressurization, 5 for HDA, and 6 for GeII) except for the pressure values 8.3 and 9.8 GPa, where we found 5 ± 1 and 6 ± 0.5, respectively.

Looking at the trend of the mean interatomic distances (upper panel) and their variances (lower panel) as a function of pressure, one can infer that an elongation of first-neighbor distances and an increase in structural disorder is associated with the onset of the LDA-HDA transition (8 GPa). By further increasing pressure, R tends to decrease as a consequence of the compression, as well as the values of σ^2, indicating that the system is more ordered. In particular, the sudden decrease of the variance around 10 GPa as well as the increase in coordination number CN are consistent with the transition to the crystalline β-Sn phase. Coordination increases gradually from the amorphous LDA (CN=4) to the crystalline phase GeII (CN=6), passing through an intermediate value in the metallic disordered phase (HDA). As discussed in the next section, this interpretation is better supported by present Raman and XAS data than the presence of a mixture of phases. Upon depressurization, we followed the sample behavior by looking at the change in the surface optical reflectivity indicating the occurrence of the phase transition. The sample has been observed to come back to its initial low reflectivity around 6 GPa. Below this pressure, we performed both XAS and x-ray diffraction (XRD) experiments. The values of R and σ^2 structural parameters and the observed diffraction lines are consistent with those of the ST12 crystalline structure (see Ref. 13). XRD peaks assigned to the ST12 phase are observed till 0.9 GPa, disappearing once the cell is open, in agreement with Raman and XAS results which indicate that the sample comes back to the LDA phase. XRD upon pressurization showed the presence

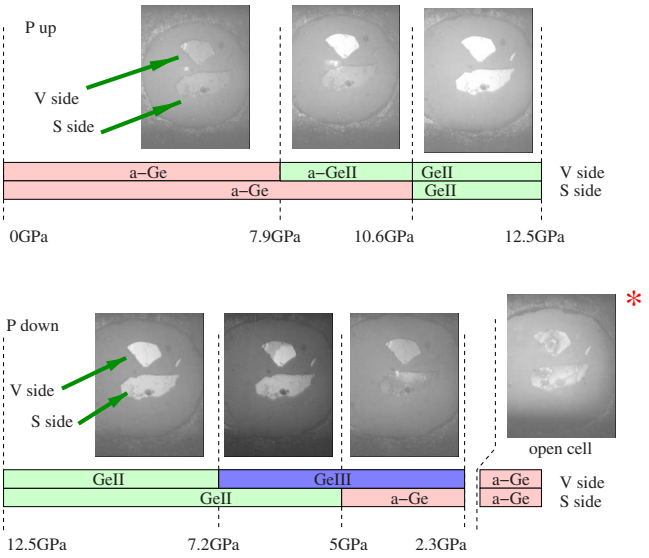

FIG. 10. (Color online) The different behaviors of the *V* and *S* side samples upon increasing and decreasing pressures are shown through the images taken during Raman measurements. The two surfaces of the sample present different transition pressures and different phases at the same pressure (indicated in the bar at the bottom of the picture), identified both from the different reflectivity of the sample and by Raman scattering. The *V* side sample becomes metallic (HDA) at lower pressures than the *S* side one and it crystallizes in the ST12 metastable structure upon depressurization around 7 GPa. The *S* side sample becomes amorphous (LDA) around 5 GPa upon depressurization, while the *V* side come back to the LDA phase only once the cell is open (depressurization from about 2 GPa to ambient pressure). The image of the sample recovered at ambient pressure is indicated by a star.

of the GeII phase above 9 GPa in different experiments, while below this pressure, only peaks assigned to the gasket and to the pressure medium could be identified.

C. Comparison of Raman and XAS results

The complex behavior of *a*-Ge films obtained upon the application of an external pressure is summarized in Fig. 10. As already discussed in Ref. 17, the morphology of the films (see Fig. 1, upper images) and the density of voids in particular plays a key role in these pressure-induced phase transitions. The close connection between morphology and metallization can be appreciated by looking at the micrographs obtained during Raman measurements and reported in Fig. 10, which show how samples characterized by different densities of voids (sides *V* and *S* of low-density *a*-Ge films, LDA) undergo different phase transitions. The LDA phase survives up to 8 GPa in the *V* side sample and up to 10.6 GPa in the *S* side sample. The *V* side LDA sample transforms to high-density amorphous Ge (HDA *a*-GeII) around 8 GPa while the *S* side sample transforms directly to the ordered GeII structure at higher pressure. As shown in the lower part of Fig. 10, the different morphology determines also a different behavior of the samples upon depressurization. The metastable ST12 crystalline phase is obtained around 7.6 GPa only in the sample characterized by low density of voids, downloading both from the disordered metallic phase (*a*-GeII) and from the ordered one (GeII). The *S* side sample becomes amorphous (LDA) around 5 GPa upon depressurization, while the *V* side comes back to the LDA phase only by opening the cell (depressurization from about 2 GPa to ambient pressure).

The succession of phase transitions observed by Raman scattering has been studied also using the x-ray absorption spectroscopy with the aim of understanding fine details of the metallization and local structural changes. The experiments described in Sec. III B show clearly the closure of the electronic gap around 8 GPa and the amount of disorder in the local structure for each observed phase. The trends in the mean distance *R* and bond variance σ^2 (see Fig. 9) show us that the transitions observed by Raman scattering and reported in Fig. 10 are fully consistent with the expected local structure of the various phases.

Moreover, XAS data were shown to be compatible with a highly disordered structure, thus confirming that the sample characterized by low density of defects undergoes a LDA-HDA phase transition. The XAS spectrum related to the HDA phase (8.3 GPa) can be possibly interpreted also as the result of a linear combination of two signals associated with two different phases, GeII and LDA. This would reflect a partial transition of sample to a more ordered structure. It is actually possible to obtain a reasonable fit of the 8.3 GPa using a two-shell model of this kind, but the obtained improvement in the residual do not justify the introduction of three more parameters. Moreover, an indication of the peculiar nature of the HDA phase comes also from the Raman-scattering patterns shown in Fig. 3. In fact, by looking at the signals of the metallic phases (bottom left of Fig. 3), we notice that those collected at pressures below 10 GPa contain traces of a vibrational spectrum in the 200–300 cm^{-1} range, while that at 12.5 GPa is flat. These features cannot be assigned to a residual LDA signal but rather to a disordered structure where first-neighbor distances are longer on average. This is a further evidence supporting our interpretation of this phase transition as a polyamorphic one.

The XAS and Raman-scattering results upon depressurization are also in quite nice agreement. In fact, XAS spectra and the corresponding structural parameters (see Fig. 9) are observed to change below about 6 GPa where Raman scattering indicates that the sample (side *V*) nucleates to the ST12 structure. Both mean distances *R* and variances σ^2 are slightly higher than in the amorphous LDA phase, as expected by the presence of ST12. Below about 2.5 GPa, those parameters coincide with those measured for the initial LDA *a*-Ge phase, again in agreement with the observations by Raman scattering discussed in Sec. III A. When available, as mentioned also in Sec. III B, XRD experiments at high pressure confirmed the present findings for the sample under consideration.

IV. CONCLUSION

In this work, we reported a detailed study on the pressure-induced transitions in amorphous Ge combining experimental techniques (Raman scattering and x-ray absorption spec-

troscopy) and theoretical *ab initio* calculations. Our samples were films of *a*-Ge obtained by evaporation and characterized by different density of voids. Experiments have been performed considering several pressure cycles in a wide pressure range up to about 17 GPa. The combined examination of Raman and XAS data elucidated the nature of the transitions undergone by our samples, both upon pressurization and depressurization.

Raman data of the GeIII (ST12) metastable phase were supported by *ab initio* (density-functional theory) calculations of the vibrational spectra. The five Raman-active peaks of the simulation performed using the GeIII experimental lattice structure are compatible with the measured spectra. The local first-neighbor distribution was obtained by Ge *K*-edge XAS analysis. Looking at the pressure trend of the mean bond distances R and variances σ^2, we have found that a characteristic elongation of R and an increase of σ^2 is obtained above 8 GPa, as a consequence of metallization. Correspondingly, the coordination number increases from 4 to 6. Upon depressurization, distances and variances below 6 GPa gradually return to the original values typical of a tetrahedral semiconductor.

The present results indicate that the amorphous specimens undergo specific and reproducible phase transitions, depending on the initial surface density of voids. Low density of void samples (side *V*) showing an LDA-HDA transition at 8 GPa and the well-known transformation to GeII at higher pressures recrystallize into the GeIII metastable phase once pressure is decreased. This structure is present in a wide pressure range (7.2–2.3 GPa). Samples characterized by higher density of voids (side *S*) transform directly to the GeII phase around 10 GPa and return to the amorphous state at 5 GPa on depressurization, as indicated by Raman spectra, which do not contain any evidence of crystalline peaks. In present experiments, amorphous films, which have crystallized upon pressure application, are always returning amorphous upon pressure release. On the contrary, originally crystalline samples recrystallize upon pressure release.

The different behavior upon pressurization and depressurization of samples characterized by different density of voids shows how morphology plays a key role in the occurrence of phase transitions. We can speculate about the relationship between the morphology and the occurrence of pressure-induced phase transition, but a precise mechanicistic model cannot be proposed on the basis of the present evidence. One possible explanation for this phenomenon could be related to the pressure-induced inhomogeneous density change and to the presence of surface stresses affecting the pressure field inside the sample. In the present experiment, the lower density of voids makes the sample locally denser, so that upon decompression, it is driven to rearrange in a denser structure, while for higher density of defects, it is likely to transform in a more open one. The present results are expected to stimulate further investigations on the role of morphology, density of voids, and inhomogeneous texture in amorphous samples undergoing pressure-induced transitions. This should be relevant not only for germanium but, also, for other semiconducting materials (e.g., silicon and GeSi alloys).

ACKNOWLEDGMENTS

We wish to acknowledge the personnel of IMPMC (Universitè Paris VI), Soleil, and University of Camerino XAS laboratories for their support in the realization of this work. The Italian MIUR (PRIN Project No. 20078F2XHX003 on densified glasses) is acknowledged for partial support of the present work.

[1] J. S. Kasper and S. M. Richards, Acta Crystallogr. **17**, 752 (1964).
[2] F. Bundy and J. S. Kasper, Science **139**, 340 (1963).
[3] A. Kailer, K. G. Nickel, and Y. G. Gogotsi, J. Raman Spectrosc. **30**, 939 (1999).
[4] M. Khayyat, G. Banini, D. G. Hasko, and M. Chaudhri, J. Phys. D **36**, 1300 (2003).
[5] G. Patriarche, E. Le Bourhis, M. Khayyat, and M. Chaudhri, J. Appl. Phys. **96**, 1464 (2004).
[6] B. Haberl, J. Bradby, M. Swain, and J. Williams, Appl. Phys. Lett. **85**, 5559 (2004).
[7] J. Jang, M. J. Lance, S. Wen, and G. M. Pharr, Appl. Phys. Lett. **86**, 131907 (2005).
[8] R. J. Nelmes, M. I. McMahon, N. G. Wright, D. R. Allan, and J. S. Loveday, Phys. Rev. B **48**, 9883 (1993).
[9] C. H. Bates, F. Dachille, and R. Roy, Science **147**, 860 (1965).
[10] O. Shimomura, S. Minomura, N. Sakai, K. Asaumi, K. Tamura, J. Fukushima, and H. Endo, Philos. Mag. **29**, 547 (1974).
[11] K. Tanaka, Phys. Rev. B **43**, 4302 (1991).
[12] J. Freund, R. Ingalls, and E. D. Crozier, J. Phys. Chem. **94**, 1087 (1990).
[13] E. Principi, A. Di Cicco, F. Decremps, A. Polian, S. De Panfilis, and A. Filipponi, Phys. Rev. B **69**, 201201(R) (2004).
[14] A. Hedler, S. L. Klaumunzer, and W. Wesch, Nature Mater. **3**, 804 (2004).
[15] M. H. Bhat, V. Molinero, E. Soignard, V. C. Solomon, S. Sastry, J. L. Yarger, and C. A. Angell, Nature (London) **448**, 787 (2007).
[16] J. Kōga, K. Nishio, T. Yamaguchi, and F. Yonezawa, J. Phys. Soc. Jpn. **73**, 388 (2004).
[17] A. Di Cicco, A. Congeduti, F. Coppari, J. C. Chervin, F. Baudelet, and A. Polian, Phys. Rev. B **78**, 033309 (2008).
[18] J. Barnett, S. Block, and J. Piermarini, Rev. Sci. Instrum. **44**, 1 (1973).
[19] F. Coppari, A. Di Cicco, A. Congeduti, J. Chervin, F. Baudelet, and A. Polian, High Press. Res. **29**, 103 (2009).
[20] A. Filipponi and A. Di Cicco, Phys. Rev. B **51**, 12322 (1995).
[21] A. Filipponi, A. Di Cicco, and C. R. Natoli, Phys. Rev. B **52**, 15122 (1995).
[22] A. Filipponi and A. Di Cicco, Phys. Rev. B **52**, 15135 (1995).
[23] P. Hohenberg and W. Kohn, Phys. Rev. **136**, B864 (1964).
[24] W. Kohn and L. Sham, Phys. Rev. **140**, A1133 (1965).
[25] S. Baroni, S. De Gironcoli, A. Dal Corso, and P. Giannozzi, Rev. Mod. Phys. **73**, 515 (2001).
[26] S. Baroni, A. Dal Corso, S. De Gironcoli, and P. Giannozzi, http://www.pwscf.org

[27] N. Troullier and J. L. Martins, Phys. Rev. B **43**, 1993 (1991).
[28] J. P. Perdew, K. Burke, and M. Ernzerhof, Phys. Rev. Lett. **77**, 3865 (1996).
[29] N. Moll, M. Bockstedte, M. Fuchs, E. Pehlke, and M. Scheffler, Phys. Rev. B **52**, 2550 (1995).
[30] A. Di Cicco, A. C. Frasini, M. Minicucci, E. Principi, J. P. Itié, and P. Munsch, Phys. Status Solidi B **240**, 19 (2003).
[31] D. Olego and M. Cardona, Phys. Rev. B **25**, 1151 (1982).
[32] J. Crain, G. J. Ackland, and S. J. Clark, Rep. Prog. Phys. **58**, 705 (1995).
[33] M. Methfessel and A. T. Paxton, Phys. Rev. B **40**, 3616 (1989).
[34] M. Lazzeri and F. Mauri, Phys. Rev. Lett. **90**, 036401 (2003).
[35] P. Brüesch, *Phonons: Theory and Experiments II* (Springer, Berlin, 1986).
[36] R. Alben, D. Weaire, J. E. Smith, and M. H. Brodsky, Phys. Rev. B **11**, 2271 (1975).
[37] C. S. Menoni, J. Z. Hu, and I. L. Spain, Phys. Rev. B **34**, 362 (1986).
[38] T. Mernagh and L. Liu, J. Phys. Chem. Solids **52**, 507 (1991).
[39] M. Hanfland and K. Syassen, High Press. Res. **3**, 242 (1990).
[40] H. Olijnyk and A. P. Jephcoat, Phys. Status Solidi B **211**, 413 (1999).